Check for updates

Steric effects in light-induced solvent proton abstraction†

Jurick Lahiri, [ID][a] Mehdi Moemeni,[a] Ilias Magoulas, [ID][a] Stephen H. Yuwono, [ID][a] Jessica Kline,[a] Babak Borhan, [ID] ⋆[a] Piotr Piecuch, [ID] ⋆[ab] James E. Jackson, [ID] ⋆[a] G. J. Blanchard [ID] ⋆[a] and Marcos Dantus [ID] ‡⋆[ab]

The significance of solvent structural factors in the excited-state proton transfer (ESPT) reactions of Schiff bases with alcohols is reported here. We use the super photobase **FR0**-SB and a series of primary, secondary, and tertiary alcohol solvents to illustrate the steric issues associated with solvent to photobase proton transfer. Steady-state and time-resolved fluorescence data show that ESPT occurs readily for primary alcohols, with a probability proportional to the relative −OH concentration. For secondary alcohols, ESPT is greatly diminished, consistent with the barrier heights obtained using quantum chemistry calculations. ESPT is not observed in the tertiary alcohol. We explain ESPT using a model involving an intermediate hydrogen-bonded complex where the proton is "shared" by the Schiff base and the alcohol. The formation of this complex depends on the ability of the alcohol solvent to achieve spatial proximity to and alignment with the **FR0**-SB* imine lone pair stabilized by the solvent environment.

Introduction

The development and characterization of reversible photo-activated reagents is central to the advancement of precision chemistry. The goal of this emerging area is to control the execution of a chemical reaction spatially and temporally through the use of photo-activated reactive chemical species. Applications for such precision chemistry are numerous, ranging from high-precision photolithography to the development of near-field chemical-reaction-based sensing and imaging of complex surfaces, including, for example, heterogeneous catalysts.

The vast majority of chemical reactions are either acid–base or redox processes, and the key to the development of precision chemistry is the ability to design photoinitiated reagents for specific purposes. Some of the best-known members of this class of molecules are photoacids and super photoacids, where

a chemical functionality on a chromophore, typically an alcohol or carboxylic acid moiety, undergoes a substantial decrease in pK_a upon photoexcitation.

Even though there are several known families of super photoacids, such as the cyanonaphthols,[1,2] only a limited number of molecules are known to function as photobases, capable of abstracting protons from alcohols. Among them are 5-methoxyquinoline[3] and (*E*)-7-((butylimino)methyl)-*N*,*N*-diethyl-9,9-dimethyl-9*H*-fluoren-2-amine (**FR0**-SB)[4] (Fig. 1) with excited-state pK_a values of 15.5 and 21, respectively. These two species are examples of molecules that exhibit excited-state intermolecular proton transfer (ESPT) rather than excited-state intramolecular proton transfer.[5,6] It is worth pointing out that unlike hydroxyquinoline, aminoquinoline, and azaindole photobases, **FR0**-SB lacks labile protons and must undergo explicit intermolecular proton transfer, as opposed to tauto-merization or other net intramolecular rearrangements. Studies carried out on 5-methoxyquinoline have concluded that a cluster of at least two solvent molecules is required to enable ESPT.[7,8] However, these investigations were not able to assess steric restrictions posed by secondary and tertiary alcohols given the fact that 5-methoxyquinoline deprotonates only low-pK_a primary alcohols (*e.g.*, halogenated ethanol).[3] To that end, we focus here on the steric properties of the solvent–solute complex, required for ESPT to occur, using the much stronger photobase **FR0**-SB as an example.

In a recent report, we presented experimental evidence for the formation of a persistent interaction between solvent primary alcohols and **FR0**-SB* based on rotational diffusion

[a] *Department of Chemistry, Michigan State University, East Lansing, MI 48824,*
USA. E-mail: babak@chemistry.msu.edu, piecuch@chemistry.msu.edu,
jackson@chemistry.msu.edu, blanchard@chemistry.msu.edu,
dantus@chemistry.msu.edu; Tel: +1-517-353-0501, +1-517-353-1151,
+1-517-353-0504, +1-517-353-1105, +1-517-353-1191

[b] *Department of Physics and Astronomy, Michigan State University, East Lansing,*
MI 48824, USA

† Electronic supplementary information (ESI) available: Experimental methods. Computational details including S_0 and S_1 total electronic energies and optimized geometries corresponding to selected points along the reaction pathways defining the excited-state proton transfer between **FR0**-SB and *n*- and i-propanol. See DOI: 10.1039/d0cp03037f

‡ Lead contact.

This journal is © the Owner Societies 2020

Phys. Chem. Chem. Phys., 2020, **22**, 19613–19622 | **19613**
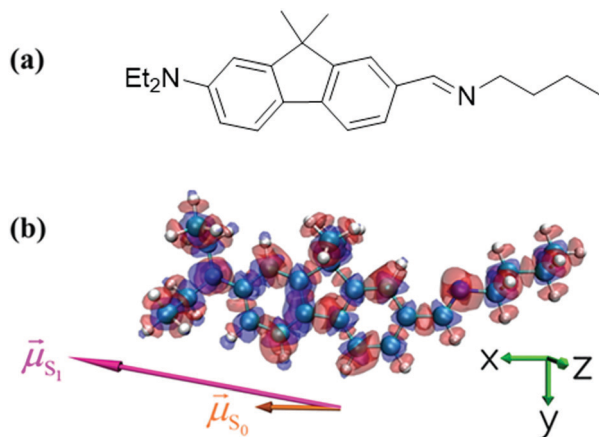
Fig. 1 The **FR0**-SB molecule and how its electronic density changes upon excitation. (a) **FR0**-SB super photobase. (b) The structure of the isolated **FR0**-SB molecule in its ground electronic S_0 state, the dipole moments characterizing the S_0 (shorter orange vector) and electronically excited S_1 (longer magenta vector) states, and the $S_1 - S_0$ total electronic density difference, resulting from the CC/EOMCC calculations described in the main text. The red/blue color indicates an increase/decrease in the electron density upon the $S_0 \rightarrow S_1$ excitation.

dynamics measurements.[9] The high-level *ab initio* calculations presented in that report, based on the coupled-cluster (CC) theory[10] and its equation-of-motion (EOM) excited-state extension,[11] indicated that this persistent interaction, which leads to ESPT, is a consequence of the *ca.* 3-fold increase in the static dipole moment of **FR0**-SB upon excitation from its ground electronic state (S_0) to its first-excited singlet state (S_1) (*cf.* Fig. 1b).[9] As shown in Fig. 1b, where we plot the $S_1 - S_0$ total electron density difference, calculated using the CC/EOMCC one-electron reduced density matrices resulting from our earlier computations,[9] the cause of this significant increase in dipole moment upon photoexcitation is an overall intramolecular migration of a relatively small amount of electron density over a long distance, from the diethylamino nitrogen to the imine nitrogen.

Even though our earlier work demonstrated that the rate of formation of the complex between **FR0**-SB* and the solvent ROH was controlled by the concentration of –OH functional groups in the solvent for primary alcohols, the details of the excited Schiff base–alcohol complex formation was left unresolved. In particular, the steric effect arising from the structure of the alcohol and the details of the associated proton-transfer reaction pathways remained unclear. Among the factors that contribute to the proton transfer process is the highly associative nature of the solvent and the role that solvent molecular structure plays in the ability to engage in an ESPT reaction with the Schiff base.

The transfer of protons between excited chromophores and their surrounding media carries different spatial and reaction coordinate implications depending on the direction of proton transfer. Photoacids require a lesser extent of solvent organization than photobases to execute the proton transfer event. Photoexcitation of photoacids leads to the ejection of a proton

from the chromophore into a highly associative bath where intermolecular proton exchange operates under an equilibrium condition. Photobases, on the other hand, require the alignment of the proton-donating solvent molecule with the excited Schiff base receptor, which is mediated by the solvent's associative network. Studies of hydroxyquinolines and azaindoles have explored the net isomerization processes in which one terminus of an excited chromophore becomes strongly basic and the other end becomes acidic, releasing a proton. In such systems, two or more alcohol molecules are needed in a hydrogen bonded "proton wire" to mediate the proton transfer process.[12–23] Much less common are photobases such as 5-methoxyquinoline or **FR0**-SB that carry no labile protons. In these systems, the above-mentioned bridging is unnecessary; the key role of the hydroxylic solvent molecules or clusters is simply to serve as a source of protons in response to the enhanced basicity engendered by photoexcitation.

The purpose of this work is to provide insights into the effect of solvent steric factors on the ESPT process. The experimental data we report are time-resolved and steady-state fluorescence measurements of **FR0**-SB in primary, secondary, and tertiary alcohols, with an emphasis on the kinetics and equilibria of the ESPT reaction. We also report the details of the ESPT reaction pathways between **FR0**-SB and representative primary and secondary alcohols predicted by quantum chemistry calculations. Our data show that primary alcohols exhibit facile proton transfer to the excited chromophore **FR0**-SB*, with secondary alcohols being much less efficient and tertiary alcohols not exhibiting measurable proton transfer. These data demonstrate collectively the existence of an intermediate complex where **FR0**-SB* and alcohol solvent molecules share the alcohol proton and mediate the ESPT process.

Results and discussion

The ability of **FR0**-SB to abstract a proton from an alcohol can be evaluated using steady-state fluorescence spectroscopy. The absorption and fluorescence spectra of **FR0**-SB dissolved in a series of solvents are shown in Fig. 2a and b. The absorption spectra are relatively independent of solvent. Fluorescence of **FR0**-SB exhibits two emission bands, one centered around 630 nm ($\sim 15\,870$ cm^{-1}) and the other near 460 nm ($\sim 21\,740$ cm^{-1}), which have been assigned to the protonated **FR0**-HSB$^+$* species and its non-protonated form **FR0**-SB*, respectively. The **FR0**-HSB$^+$* emission band appears as a result of ESPT.[4] Fluorescence spectra have been divided by the frequency cubed, according to the transition dipole representation, which makes fluorescence intensity proportional to the population of emitters according to the Einstein coefficient of spontaneous emission.[24] In Fig. 2a we have normalized the protonated emission intensities for all solvents allowing a facile comparison of the extent of ESPT for **FR0**-SB* as a function of solvent alcohol identity.

Shown in Fig. 2b is the normalized absorption and fluorescence spectra of **FR0**-SB in primary, secondary, and tertiary alcohols. Included is acetonitrile, an aprotic solvent, which is

19614 | *Phys. Chem. Chem. Phys.*, 2020, **22**, 19613–19622

This journal is © the Owner Societies 2020
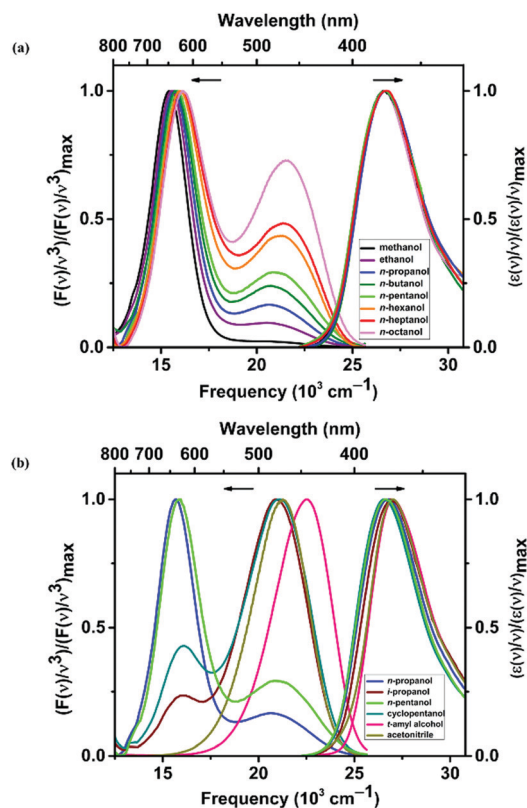
Fig. 2 Steady-state absorption and fluorescence spectra of **FR0**-SB in alcohols. (a) The normalized absorption and emission spectra of **FR0**-SB in primary alcohols from methanol to n-octanol. (b) The absorption and emission spectra of **FR0**-SB in various solvents to compare steric hindrance. The long wavelength emission near 630 nm ($\sim$15 870 cm^{-1}) corresponds to **FR0**-HSB^{+}*, while the short wavelength emission near 460 nm ($\sim$21 740 cm^{-1}) corresponds to **FR0**-SB*.

Table 1 Analysis of the steady-state spectroscopy results. Relative −OH concentration for the different alcohols, K_{eq} obtained as the ratio between **FR0**-SB* and **FR0**-HSB^{+}*, and derived ΔG^0 values for proton abstraction from steady-state data

Solvent[a]	[−OH] (M)	$K_{eq} \approx \dfrac{[\textbf{FR0}\text{-HSB}^{+*}]}{[\textbf{FR0}\text{-SB}^*]}$	ΔG^0 (kJ mol^{-1})
MeOH	24.7	35.6 ± 3.0	−8.7 ± 0.2
EtOH	17.0	7.6 ± 0.5	−4.9 ± 0.2
n-PrOH	13.4	3.5 ± 0.1	−3.1 ± 0.1
n-BuOH	10.9	2.5 ± 0.1	−2.2 ± 0.1
n-PeOH	9.2	2.0 ± 0.1	−1.7 ± 0.1
n-HxOH	8.0	1.6 ± 0.1	−1.1 ± 0.1
n-HpOH	7.0	1.4 ± 0.1	−0.9 ± 0.1
n-OcOH	6.4	1.1 ± 0.1	−0.2 ± 0.1
i-PrOH	13.1	0.2 ± 0.1	4.2 ± 0.1
c-PeOH	11.0	0.3 ± 0.1	2.6 ± 0.1
TAA	9.2	—	—
ACN	—	—	—

[a] Abbreviations: MeOH = methanol, EtOH = ethanol, n-PrOH = n-propanol, n-BuOH = n-butanol, n-PeOH = n-pentanol, n-HxOH = n-hexanol, n-HpOH = n-heptanol, n-OcOH = n-octanol, i-PrOH = i-propanol, c-PeOH = cyclopentanol, TAA = t-amyl alcohol, ACN = acetonitrile.

not capable of undergoing ESPT and thus exhibits no **FR0**-HSB^{+}* emission. Fluorescence spectra are normalized to the most intense emission intensity to facilitate comparison of the extent of ESPT by **FR0**-SB* in the selected solvents. We find a substantial decrease in the probability of ESPT relative to the primary alcohols for secondary alcohols (i-propanol and cyclopentanol) and observe no ESPT emission in the case of the tertiary alcohol t-amyl alcohol (TAA).

The ratio of the areas of the two emission bands for a given solvent can be used to estimate the fraction of **FR0**-SB that undergoes ESPT, after correction for the fluorescence quantum yields (Φ_{fl}) of the non-protonated and protonated species.[4] Fluorescence measurements were taken in acetonitrile and acidified acetonitrile to quantify the difference in Φ_{fl} for **FR0**-SB* and **FR0**-HSB^{+}*. This comparison was repeated with acetone as the solvent to obtain the ratio of Φ_{fl} for the non-protonated to protonated forms of **FR0**-SB in a different solvent system. The unprotonated species **FR0**-SB* exhibits a 1.5 times greater Φ_{fl} than **FR0**-HSB^{+}*, in agreement with previous results.[4] However, here we use the transition-dipole representation to ensure emission is proportional to the number of emitters.[24] Table 1 summarizes the equilibrium constant and free energy of proton abstraction data as a function of solvent.

For the primary alcohol solvents there is a monotonic decrease in **FR0**-HSB^{+}* fluorescence intensity with increasing solvent aliphatic chain length, which is directly proportional to solvent [−OH].[9] Secondary alcohols exhibit a markedly reduced propensity for proton donation relative to that seen for primary alcohols, despite the fact that the pK_a values of primary and secondary alcohols, differing by structural isomerism, are similar (e.g., pK_a = 16.1 for n-propanol[25] and 16.5 for i-propanol[26]). We note that cyclopentanol has a higher protonation probability than i-propanol despite the lower −OH concentration. The tertiary alcohol TAA appears to not participate in ESPT to within our ability to detect **FR0**-HSB^{+}*. Assuming that **FR0**-SB* and **FR0**-HSB^{+}* are in equilibrium, we can derive the free energy of the process.

$$\textbf{FR0}\text{-SB}^* + \text{ROH} \underset{}{\overset{K_{eq}}{\rightleftharpoons}} \textbf{FR0}\text{-HSB}^{+*} + \text{RO}^- \tag{1}$$

$$\Delta G^0 = -RT \ln K_{eq}$$
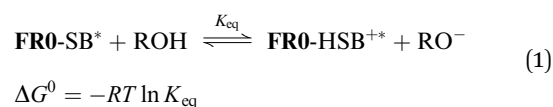
The free energy values derived from the steady-state data are included in Table 1.

In addition to the steady-state measurements, we also performed picosecond time-resolved fluorescence lifetime measurements for **FR0**-SB* and **FR0**-HSB^{+}* in the same solvents to relate the population relaxation dynamics of these species to the ESPT process. Fig. 3a shows the emission decay of **FR0**-SB* for the series of linear alcohols, where a monotonic increase in fluorescence lifetime was observed with increasing solvent aliphatic chain length. Fig. 3b shows the same emission decay data for **FR0**-SB* in selected primary, secondary, and tertiary alcohols. There is a significantly longer fluorescence lifetime for **FR0**-SB* decay in secondary and tertiary alcohols, suggesting less efficient proton abstraction from the alcohol in these media. For comparison, the decay of **FR0**-SB* in acetonitrile, which is incapable of participating in proton transfer, is also

This journal is © the Owner Societies 2020

Phys. Chem. Chem. Phys., 2020, **22**, 19613–19622 | **19615**
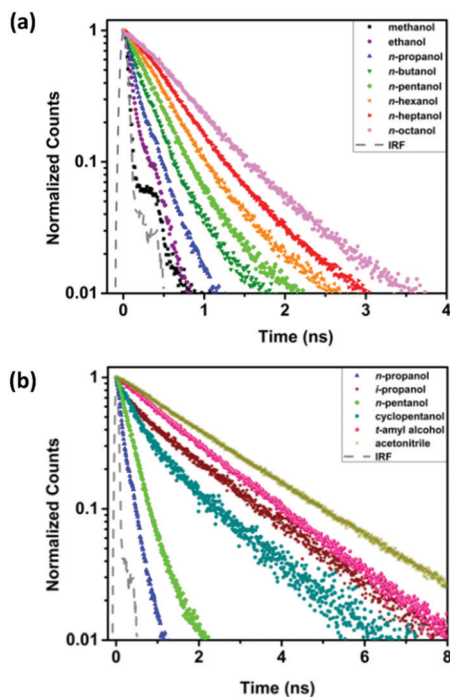
Fig. 3 The fluorescence decay responses plotted on a $\log_{10}$ scale of **FR0**-SB* detected at 460 nm in (a) primary alcohols and (b) selected primary, secondary, and tertiary alcohols. The fitting function used was $f(t) = a_1 \exp(-t/\tau_{SB1}) + a_2 \exp(-t/\tau_{SB2})$. For the time constants reported in Table 2, the IRF has been deconvoluted using a convolute-and-compare method.
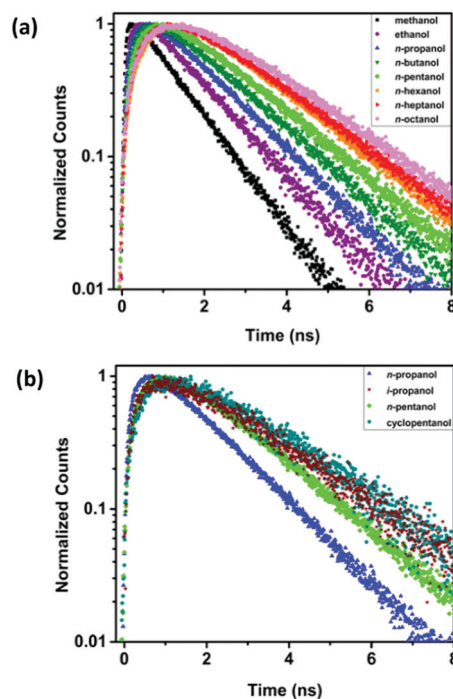
Fig. 4 The fluorescence decay responses plotted on a $\log_{10}$ scale of **FR0**-HSB$^+$* detected at 630 nm in (a) primary alcohols and (b) selected primary and secondary alcohols. The fitting function used was $f(t) = b_1 \exp(-t/\tau_{HSB}) - b_2 \exp(-t/\tau_X)$. For the time constants reported in Table 2, the IRF has been deconvoluted using a convolute-and-compare method.

shown in Fig. 3b. The trends observed in the primary alcohols can be understood in terms of the relative concentration of –OH in each solvent.[9] The time-resolved emission increase and subsequent decay for **FR0**-HSB$^+$* in the primary alcohols, methanol through *n*-octanol, is shown in Fig. 4a. A monotonic increase in the time constants of both processes with increasing solvent aliphatic chain length is evident. The data in Fig. 4b provide a comparison of the time-resolved emission transients for **FR0**-HSB$^+$* for selected primary and secondary alcohols. Because the extent of ESPT for tertiary alcohols is beneath the detection limit, there are no data for **FR0**-HSB$^+$* in TAA.

The time constants for the processes discussed above are summarized in Table 2. As expected, linear alcohols exhibit a smooth trend. Secondary alcohols show significantly longer lifetimes, indicating lower probability for proton transfer. In the case of cyclopentanol, we observe a faster **FR0**-SB* decay than for i-propanol, suggesting a slightly higher probability of proton transfer, in agreement with the steady-state emission spectroscopic data (Fig. 2b). It is important to note that cyclopentanol shows a slower rise of **FR0**-HSB$^+$* emission as compared to i-propanol. This finding is currently under investigation and may provide insight into the details of the reaction coordinate for proton transfer in secondary alcohols.

Our analysis of the time-resolved data is based on a kinetic scheme used in our previous work involving linear alcohols,[9] modified slightly and schematized in Fig. 5. The excitation function, $\delta(t)$, is a *ca.* 5 ps for the 350 nm laser pulse, which

produces the electronically excited **FR0**-SB* molecule. The photoexcited chromophore, **FR0**-SB*, relaxes either radiatively back to **FR0**-SB (τ_{SB2}, $\lambda_{em} \approx 460$ nm) or non-radiatively, along a reaction coordinate on the excited-state potential energy surface, producing an intermediate complex [**FR0**-SB*···H–OR] in the early stages of the ESPT process. This complex undergoes a transformation that results in proton abstraction from the alcohol and formation of the **FR0**-HSB$^+$* and $^-$OR products (τ_X). Emission from the protonated **FR0**-HSB$^+$* species near 630 nm competes with deprotonation (τ_{HSB}).

Considering τ_X and τ_{HSB} as lifetimes that reflect the protonation and deprotonation processes in the equilibrium between the intermediate complex [**FR0**-SB*···H–OR] and **FR0**-HSB$^+$*, then the ratio of the time constants τ_X/τ_{HSB} (Fig. 6a) can be compared to the free energy values (Table 1) derived from the steady-state band intensity ratio (Fig. 6b). The correspondence between steady-state and time-resolved measurements provides confidence in assigning an equilibrium between the intermediate and the protonated species. However, the free energy for the process cannot be derived from the latter equilibrium given the existence of the intermediate. The large deviation observed for the secondary alcohols in Fig. 6a does not translate into a difference in the time domain data in Fig. 6b. We consider this as an indication that formation of the transient solvent organization required for proton transfer is more challenging on structural grounds for secondary alcohols than it is for the primary ones.

Table 2 Fluorescence lifetimes obtained from time-correlated single photon counting experiments. The time constants are as defined in Fig. 5. Uncertainties are $\pm\sigma$. The χ^2 values across all fits were below 0.47

Solvent[a]	a_1	τ_{SB1} (ps)	a_2	τ_{SB2} (ps)	$\bar{\tau}_{SB}$[b] (ps)	τ_X (ps)	τ_{HSB} (ps)
MeOH	0.99	18 ± 8	0.01	478 ± 185	23 ± 9	42 ± 4	1050 ± 10
EtOH	0.93	57 ± 6	0.07	232 ± 26	68 ± 15	150 ± 5	1280 ± 10
n-PrOH	0.92	104 ± 15	0.08	463 ± 38	134 ± 22	244 ± 4	1470 ± 10
i-PrOH	0.70	110 ± 16	0.30	1760 ± 20	612 ± 13	375 ± 24	2290 ± 50
n-BuOH	0.86	147 ± 5	0.14	504 ± 23	198 ± 13	391 ± 5	1610 ± 30
n-PeOH	0.90	272 ± 35	0.10	1040 ± 80	347 ± 53	589 ± 8	1630 ± 20
c-PeOH	0.74	231 ± 6	0.26	1580 ± 30	582 ± 17	630 ± 32	2200 ± 10
n-HxOH	0.94	336 ± 51	0.06	1420 ± 240	401 ± 141	755 ± 13	1640 ± 30
n-HpOH	0.97	470 ± 8	0.03	1690 ± 120	502 ± 137	749 ± 7	1800 ± 10
n-OcOH	0.95	536 ± 8	0.05	1850 ± 90	602 ± 50	846 ± 18	1870 ± 20

[a] Abbreviations: MeOH = methanol, EtOH = ethanol, n-PrOH = n-propanol, i-PrOH = i-propanol, n-BuOH = n-butanol, n-PeOH = n-pentanol, c-PeOH = cyclopentanol, n-HxOH = n-hexanol, n-HpOH = n-heptanol, n-OcOH = n-octanol. [b] $\bar{\tau}_{SB} = a_1\tau_{SB1} + a_2\tau_{SB2}$.
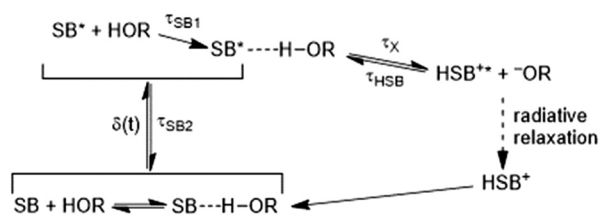
Fig. 5 Kinetic model for the ESPT reaction between **FR0**-SB and the alcohol solvent ROH.

The data plotted in Fig. 6b make it clear that secondary alcohols deviate drastically from the linear trend observed for primary alcohols as a function of [–OH], underscoring the important role of solvent molecular structure in the proton abstraction reaction. We postulate that for secondary alcohols the initial formation of an excited Schiff base–solvent complex may be an activated process, which is a testable hypothesis. The extent of proton abstraction in n- and i-propanol as a function of temperature was measured, following excitation at 430 nm, in order to minimize the excess energy in the excited state; these measurements were corrected by the independently measured change in fluorescence quantum yield as a function of temperature. The results from these measurements are shown in Fig. 7a with the equilibrium constants and the free energy of protonation values listed in Table 3. We observe no significant temperature dependence for n-propanol, but do observe a decrease in proton abstraction in i-propanol with increasing temperature. Table 4 and Fig. 7b show the lifetimes of **FR0**-SB* as a function of temperature for the n- and i-propanol. These data suggest that conversion of **FR0**-SB* to **FR0**-HSB^{+}* along the reaction coordinate resulting in the deprotonation of n-propanol is a process characterized by a low-energy barrier, which is lower than the analogous process with i-propanol. No discernable temperature-dependent changes were observed in the absorption spectra for **FR0**-SB in these two solvents (not shown), consistent with the protonation occurring exclusively in the excited electronic state.

While explicit thermodynamic information is not extracted from the above data, given the existence of an intermediate, it is clear that the negative slope of the temperature dependence shown in Fig. 7a implies a distinctly negative entropy term for ESPT in the case of the secondary alcohol, with entropic factors being less significant for the primary ones. This finding is consistent with the proton transfer reaction coordinate depending on a solvent configuration that is more difficult to access on steric grounds for the secondary alcohol than for the primary alcohol. It is important to note that τ_X is longer than τ_{SB1} for both primary and secondary alcohols, implying the existence of an intermediate state between **FR0**-SB* and **FR0**-HSB^{+}*, originally postulated by Lahiri et al.[9] and consistent with the scheme shown in Fig. 5.
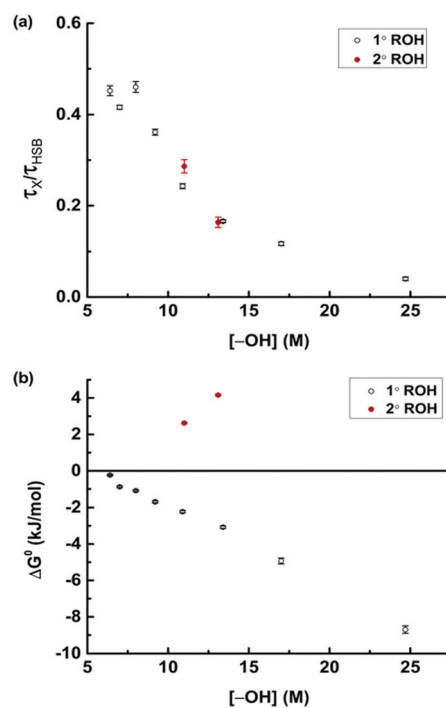
Fig. 6 Trends in dynamics and free energy as a function of relative [–OH]. (a) The ratio of the time constants τ_X and τ_{HSB} is plotted as a function of relative [–OH]. (b) ΔG^0 for proton abstraction obtained from the ratio of **FR0**-SB* to **FR0**-HSB^{+}* emission as a function of relative [–OH]. We note good agreement between the time-resolved and the steady-state data for the linear alcohols.
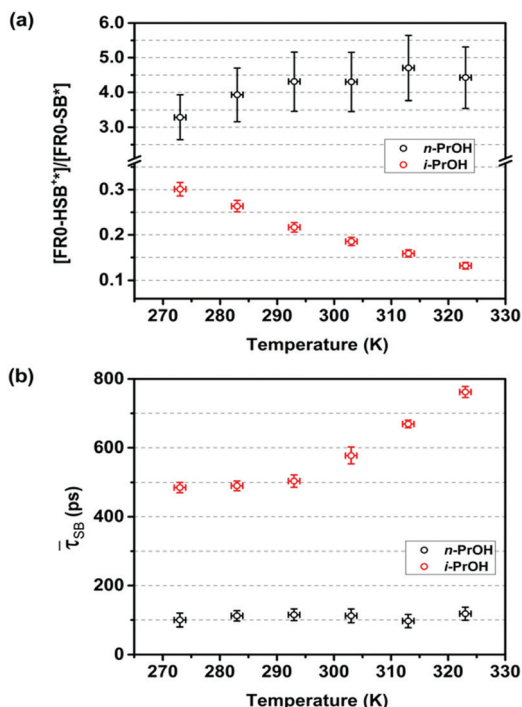
Fig. 7 Temperature-dependent proton transfer data for *n*- and i-propanol. (a) Concentration ratio of the protonated and unprotonated **FR0**-SB* following photoexcitation obtained from steady-state spectra. (b) Temperature-dependent $\bar{\tau}_{SB}$ for **FR0**-SB* obtained from time-resolved measurements. From these steady-state band ratio data, we can determine the temperature-dependent equilibrium constant for protonation/deprotonation of **FR0**-SB*.

Table 3 Temperature-dependent steady-state data in *n*-propanol (*n*-PrOH) and i-propanol (i-PrOH)

Solvent	T (K)	$K_{eq} \approx \dfrac{[\textbf{FR0}\text{-HSB}^{+*}]}{[\textbf{FR0}\text{-SB}^{*}]}$	ΔG^0 (kJ mol^{-1})
n-PrOH	273 ± 1	3.3 ± 0.6	−2.7 ± 0.4
	283 ± 1	3.9 ± 0.8	−3.2 ± 0.5
	293 ± 1	4.3 ± 0.9	−3.6 ± 0.5
	303 ± 1	4.3 ± 0.8	−3.7 ± 0.5
	313 ± 1	4.7 ± 0.9	−4.0 ± 0.5
	323 ± 1	4.4 ± 0.9	−4.0 ± 0.5
i-PrOH	273 ± 1	0.25 ± 0.01	3.1 ± 0.1
	283 ± 1	0.22 ± 0.01	3.5 ± 0.1
	293 ± 1	0.18 ± 0.01	4.2 ± 0.1
	303 ± 1	0.15 ± 0.01	4.7 ± 0.1
	313 ± 1	0.13 ± 0.01	5.2 ± 0.1
	323 ± 1	0.11 ± 0.01	5.9 ± 0.1

The issue that is central to understanding the light-induced proton abstraction reactions examined in this work is whether or not there is a resolvable intermediate [**FR0**-SB*···H–OR] complex along the reaction coordinate that undergoes the ESPT leading to the formation of the [**FR0**-HSB^{+*}···$^-$OR] product. To address this issue and to provide deeper insights into the role of steric effects in the proton transfer reactions between the excited **FR0**-SB* chromophore and alcohol solvent molecules, we augmented the experimental effort by performing electronic

structure calculations focusing on the ground, S$_0$, and first-excited singlet, S$_1$, electronic states of the solvated **FR0**-SB system. In the calculations reported in this work, we focused on the reactions of **FR0**-SB* with *n*- and i-propanol. The *n*- and i-propanol molecules are the smallest alcohol species in the primary and secondary categories considered in our experiments that permit structural isomerism.

In modeling the ESPT process, we considered the interaction between **FR0**-SB* and a cluster of three alcohol molecules, which, according to our computations, is the minimum number of explicit solvent molecules necessary for the proton transfer to occur. In trying to use complexes consisting of **FR0**-SB* bound to fewer alcohol molecules, our calculations could not detect the presence of the second minimum corresponding to ESPT. The remaining, *i.e.*, bulk, solvation effects were incorporated using the universal continuum solvation model based on solute electron density (SMD).[27] For the details of our electronic structure computations, which were based on density functional theory and its time-dependent extension to excited states, see the ESI.†

In constructing the reaction pathways characterizing the proton transfer between **FR0**-SB* and *n*- and i-propanol, the following protocol was adopted. For each of the two alcohols, the geometries of the electronically excited reactant and product complexes were optimized. The reactant complex is the **FR0**-SB* chromophore hydrogen-bonded to the cluster of three solvent molecules, *i.e.*, the [**FR0**-SB*···HOR] species with two ROH molecules attached to the alcohol bonded to **FR0**-SB*. The product of the proton transfer reaction is the [**FR0**-HSB^{+*}···$^-$OR] complex with two ROH molecules attached to it. Having established the internuclear distances between the proton being transferred and the imine nitrogen of **FR0**-SB* in the reactant and the product complexes, designated in Fig. 8 as r_1 and r_2, respectively, we probed the [**FR0**-SB*···HOR] → [**FR0**-HSB^{+*}···$^-$OR] reaction pathway by introducing an equidistant grid of N–H separations using the step size defined as $(r_1 - r_2)/10$. The molecular structure at each point along the above ESPT reaction pathway was obtained by freezing the N–H distance at the respective grid value and reoptimizing the remaining geometrical parameters. We also optimized the geometry of **FR0**-SB hydrogen-bonded to the cluster of three alcohol molecules in the ground electronic state, needed to calculate the S$_0$ → S$_1$ vertical excitation energy. The complete set of Cartesian coordinates defining the molecular structures along the ESPT reaction pathways obtained in this work and the corresponding S$_0$ and S$_1$ total electronic energies can be found in the ESI.†

The results of our quantum chemistry computations, shown in Fig. 9–11, reveal the intricacies of the excited-state proton abstraction process initiated by the formation of the [**FR0**-SB*···H–OR] complex. In Fig. 9, we present the calculated minimum-energy pathways characterizing the ESPT reactions involving **FR0**-SB in its first-excited singlet S$_1$ state and the *n*- and i-propanol molecules along the internuclear distance between the imine nitrogen of **FR0**-SB and the proton being transferred. For completeness, the energetics characterizing the corresponding S$_0$ ground states as well as the S$_0$ and S$_1$

19618 | *Phys. Chem. Chem. Phys.*, 2020, **22**, 19613–19622

This journal is © the Owner Societies 2020

Table 4 Temperature-dependent fluorescence lifetimes in n-propanol (n-PrOH) and i-propanol (i-PrOH) obtained from time-correlated single photon counting experiments. Uncertainties are $\pm\sigma$. The χ^2 values across all fits were below 0.4

Solvent	T (K)	a_1	τ_{SB1} (ps)	a_2	τ_{SB2} (ps)	$\bar{\tau}_{SB}{}^a$ (ps)	τ_X (ps)	τ_{HSB} (ps)
n-PrOH	273 ± 1	0.94	80 ± 10	0.06	420 ± 30	100 ± 20	220 ± 10	2560 ± 20
	283 ± 1	0.93	90 ± 10	0.07	450 ± 20	112 ± 15	210 ± 10	2360 ± 20
	293 ± 1	0.91	86 ± 8	0.09	392 ± 28	115 ± 17	181 ± 4	2250 ± 20
	303 ± 1	0.95	86 ± 9	0.05	562 ± 34	112 ± 20	160 ± 5	2230 ± 30
	313 ± 1	0.94	67 ± 5	0.06	582 ± 33	97 ± 19	133 ± 3	2400 ± 20
	323 ± 1	0.96	82 ± 6	0.04	894 ± 26	118 ± 19	110 ± 6	2380 ± 10
i-PrOH	273 ± 1	0.75	116 ± 5	0.25	1590 ± 20	485 ± 15	258 ± 8	3050 ± 20
	283 ± 1	0.75	111 ± 11	0.25	1640 ± 20	490 ± 14	233 ± 8	3070 ± 30
	293 ± 1	0.75	102 ± 6	0.25	1710 ± 30	504 ± 18	199 ± 11	3070 ± 30
	303 ± 1	0.72	95 ± 13	0.28	1820 ± 30	578 ± 24	160 ± 5	2970 ± 10
	313 ± 1	0.68	101 ± 8	0.32	1860 ± 10	669 ± 11	127 ± 6	3090 ± 20
	323 ± 1	0.63	101 ± 11	0.37	1890 ± 20	762 ± 16	106 ± 9	2940 ± 30

^{a} $\bar{\tau}_{SB} = a_1\tau_{SB1} + a_2\tau_{SB2}$.
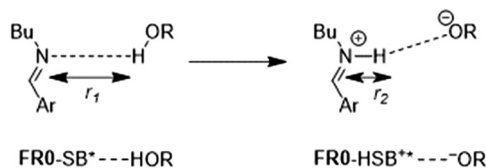
Fig. 8 Schematic representation of the r_1 and r_2 N–H internuclear distances needed to create the grid defining the ESPT reaction pathway.

energies obtained at the optimized ground-state structures of the relevant [**FR0**-SB···HOR] complexes are also provided (the leftmost points in Fig. 9). As shown in Fig. 9, the ground-state energy monotonically increases as the alcohol proton approaches the imine nitrogen of **FR0**-SB, indicating that the proton abstraction occurs in the excited state of **FR0**-SB, not in the ground state, in agreement with the experimental observations. As elaborated on above, in the experiments reported in this work, the excited state of **FR0**-SB is populated by photoabsorption from the ground
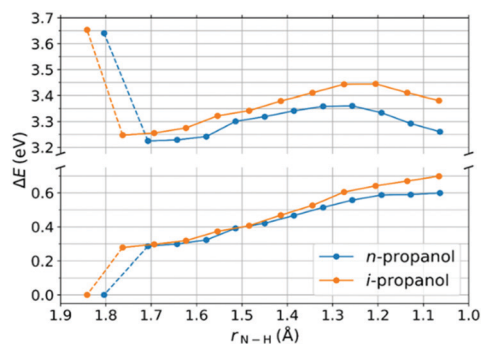
Fig. 9 Results from the reaction pathway calculations showing ground- and excited-state energy differences as a function of proton abstraction. The SMD/CAM-B3LYP/6-31+G* ground-state (S$_0$) and excited-state (S$_1$) reaction pathways corresponding to the proton abstraction from n-propanol (blue) and i-propanol (orange) by **FR0**-SB along the internuclear distance between the imine nitrogen and the alcohol proton being transferred (see the ESI† for the computational details). The energies ΔE are shown relative to the ground-state minimum of the respective pathways. The dashed line in each pathway indicates the excited-state geometry relaxation following the S$_0$ → S$_1$ excitation of **FR0**-SB.

electronic state. Our calculated S$_0$ → S$_1$ excitation energies of **FR0**-SB in n- and i-propanol of ~3.6 eV agree quite well with their corresponding experimental values of ~3.3 eV (see Fig. 2b and 9–11). Upon relaxing the excited-state geometries (see the dashed lines in Fig. 9), the difference in the behavior of the bulkier i-propanol species in the [**FR0**-SB*···HOR] complex relative to its n-propanol counterpart becomes apparent already in the early stages of the deprotonation process. In particular, the internuclear distance between the imine nitrogen of **FR0**-SB and the alcohol proton that is hydrogen-bonded to it is ~0.1 Å larger in i-propanol than in n-propanol (cf. Fig. 9–11). Furthermore, Fig. 9 reveals that even though the ESPT process takes place in both n- and i-propanol, the barrier height characterizing the reaction involving the secondary alcohol i-propanol species is ~50% higher than the analogous barrier associated with its primary alcohol n-propanol counterpart, consistent with the larger distance between the proton being transferred and the oxygen of the alcohol in i-propanol relative to that in n-propanol in the corresponding transition states (see Fig. 10 and 11). At the same time, the barrier for the reverse process, i.e., deprotonation of **FR0**-HSB^{+*}, in i-propanol is about 35% lower than that characterizing the analogous process in n-propanol.

At first glance, the observed decrease in ESPT as a function of increasing temperature seems to contradict the need to overcome a higher-energy barrier, but there is no contradiction here. Indeed, as the thermal energy of the system is increased, the individual solvent molecules spend less and less time oriented along the reaction coordinate, resulting in a decrease in the efficiency of proton transfer. This explanation implies that in order for the ESPT to occur, the intermediate [**FR0**-SB*···HOR] complex involving the alcohol molecule, with the additional alcohol molecules around it, must achieve spatial proximity and alignment of the alcohol's –OH group with the **FR0**-SB* imine lone pair, shown in Fig. 10 and 11. These steric requirements for the formation of the intermediate [**FR0**-SB*···HOR] complex result in a large negative entropy component. Our analysis of the temperature-dependent data corroborates the large negative entropy associated with i-propanol.

The reluctance of **FR0**-SB* to abstract protons from branched (secondary) alcohols, such as i-propanol, despite the similarity of

This journal is © the Owner Societies 2020

Phys. Chem. Chem. Phys., 2020, **22**, 19613–19622 | **19619**
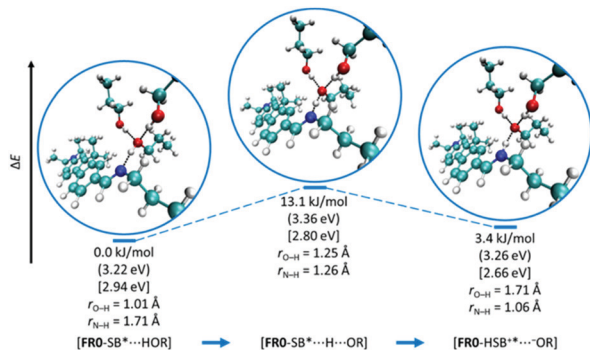
Fig. 10 Snapshots of the proton abstraction process from *n*-propanol. The SMD/CAM-B3LYP/6-31+G* optimized geometries of the [**FR0**-SB*···HOR] reactant, [**FR0**-SB*···H···OR] transition state, and [**FR0**-HSB⁺*···⁻OR] product of the ESPT process between **FR0**-SB in its S_1 electronic state and three *n*-propanol molecules (see the ESI† for the computational details). The ΔE values in kJ mol⁻¹ are given relative to the reactant energy. The energies inside parentheses, in eV, are given relative to the [**FR0**-SB···HOR] minimum in the ground electronic state S_0, while those inside square brackets correspond to the S_0–S_1 vertical transitions at each respective geometry. The r_{O-H} and r_{N-H} distances at each geometry represent the internuclear separations between the proton being transferred and the oxygen of *n*-propanol and the imine nitrogen of **FR0**-SB, respectively.
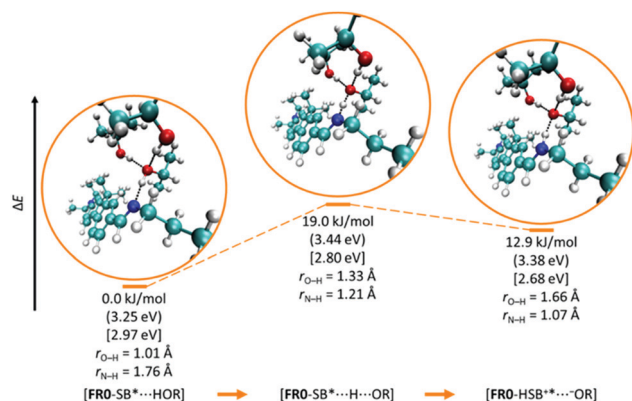
Fig. 11 Snapshots of the proton abstraction process from i-propanol. The SMD/CAM-B3LYP/6-31+G* optimized geometries of the [**FR0**-SB*···HOR] reactant, [**FR0**-SB*···H···OR] transition state, and [**FR0**-HSB⁺*···⁻OR] product of the ESPT process between **FR0**-SB in its S_1 electronic state and three i-propanol molecules (see the ESI† for the computational details). The ΔE values in kJ mol⁻¹ are given relative to the reactant energy. The energies inside parentheses, in eV, are given relative to the [**FR0**-SB···HOR] minimum in the ground electronic state S_0, while those inside square brackets correspond to the S_0–S_1 vertical transitions at each respective geometry. The r_{O-H} and r_{N-H} distances at each geometry represent the internuclear separations between the proton being transferred and the oxygen of i-propanol and the imine nitrogen of **FR0**-SB, respectively.

its bulk properties (*e.g.*, dielectric constant, viscosity, pK_a) to *n*-propanol, appears to be a consequence of steric factors that may significantly affect the initial formation of the [**FR0**-SB*···HOR] complex. The higher degree of solvent organization required to accomplish ESPT in i-propanol, as observed in Fig. 11, results in a

negative entropy contribution that leads to the reduced proton transfer yield, as reflected in the temperature-dependent weighted protonation time data in i-propanol (Fig. 7 and Table 4). The inability of **FR0**-SB* to form a complex with TAA is consistent with a steric explanation of our findings. ESPT requires proximity of the hydroxyl group to the imine group of the photobase.

Our calculations summarized in Fig. 10 and 11 imply that there is a need for a complex with two hydrogen bonds to the –OH group of the alcohol that transfers the proton. This "branched" arrangement is unusual; X-ray diffraction structures of the *n*-alkanols ethanol and butanol, congeners of *n*-propanol, show only linear structures of –OH moieties, in which each oxygen accepts only one hydrogen bond.[28,29] However, the "structure" of *n*-propanol in the liquid phase has been studied and consists of chains of various lengths with modest amounts (a few percent) of branching.[30–32] For i-propanol, which has a stronger preference for cyclic clusters, such configurations are unlikely and again, are not observed in the crystal structure of the pure solvent.[33]

Indeed, for both *n*- and i-propanol, our computations predict the linear alcohol clusters to be about 8–12 kJ mol⁻¹ lower in energy compared to the branched arrangements, not only for the ground-state [**FR0**-SB···HOR] species, but also in the case of the [**FR0**-SB*···HOR] ESPT reactant. Nevertheless, the situation changes dramatically, in favor of the branched alcohol conformations, when one considers the [**FR0**-HSB⁺*···⁻OR] product of the ESPT reaction. In the case of *n*-propanol, for example, the branched [**FR0**-HSB⁺*···⁻OR] structure is lower in energy than the linear one by about 2 kJ mol⁻¹. This is related to the fact that the branched alcohol arrangement solvates the RO⁻ species more effectively. Consequently, the $E_{product} - E_{reactant}$ energy difference in the case of the linear *n*-propanol configuration, of 14.3 kJ mol⁻¹, is higher than the 13.1 kJ mol⁻¹ activation barrier characterizing the branched conformation (see Fig. 10), implying that the activation energy characterizing the linear arrangement is even larger. The difference between the branched and linear conformations is pronounced even more when one considers i-propanol. In this case, the $E_{product} - E_{reactant}$ energy difference in the linear cluster is about 8 kJ mol⁻¹ higher than the activation barrier characterizing the branched arrangement (*cf.* Fig. 11). Based on our calculations we can conclude that the branched structures adopted in modeling of the ESPT reactions, while unusual in the case of the pure solvents, are a more realistic representation of the [**FR0**-SB*···HOR] → [**FR0**-HSB⁺*···⁻OR] process, since they lead to smaller activation energies compared to the linear arrangements of alcohol molecules bound to **FR0**-SB*. Last, but not least, the difficulty in achieving the configurations shown in Fig. 11 is consistent with the greatly diminished protonation yield observed for i-propanol and the lack of protonation observed for tertiary alcohols.

Conclusions

We have reported on the ESPT dynamics in the reactions of the super photobase **FR0**-SB with a wide variety of alcohol solvents.

Steady-state and time-resolved fluorescence spectroscopy data from a series of primary, secondary, and tertiary alcohols, combined with carefully calibrated quantum chemistry calculations, demonstrate that the efficiency of solvent proton abstraction by the electronically excited **FR0**-SB* species depends on the alcohol structure. Our results for **FR0**-SB, a photobase lacking labile protons, are in contrast with those obtained for azaindole and quinoline photobases, where the distance between a labile proton in the molecule and the protonation site is at most three bond-lengths away. While for primary alcohols the efficiency of proton abstraction by **FR0**-SB* displays a simple –OH concentration-dependence, the efficiency of proton abstraction from secondary alcohols is largely determined by steric factors preventing the formation of reactive solvent configurations, in agreement with the barrier heights resulting from quantum chemistry calculations. Proton transfer from solvent to **FR0**-SB* is not detectable in the tertiary *t*-amyl alcohol, which strengthens the validity of our analysis emphasizing the significance of steric factors further. Our experimental and theoretical results show that a pre-requisite for proton transfer is the formation of an intermediate [**FR0**-SB*···HOR] complex. They also suggest that in order for the ESPT to occur, the [**FR0**-SB*···HOR] complex must achieve spatial proximity between the **FR0**-SB* and HOR fragments and alignment of the alcohol's –OH group with the **FR0**-SB* imine lone pair, stabilized by solvation effects.

Conflicts of interest

There are no conflicts to declare.

Acknowledgements

References

1 K. M. Solntsev, D. Huppert and N. Agmon, *J. Phys. Chem. A*, 1999, **103**, 6984–6997.

2 K. M. Solntsev, D. Huppert, N. Agmon and L. M. Tolbert, *J. Phys. Chem. A*, 2000, **104**, 4658–4669.

3 J. R. Hunt and J. M. Dawlaty, *J. Phys. Chem. A*, 2018, **122**, 7931–7940.

4 W. Sheng, M. Nairat, P. D. Pawlaczyk, E. Mroczka, B. Farris, E. Pines, J. H. Geiger, B. Borhan and M. Dantus, *Angew. Chem., Int. Ed.*, 2018, **57**, 14742–14746.

5 T. Yatsuhashi and H. Inoue, *J. Phys. Chem. A*, 1997, **101**, 8166–8173.

6 M. Ekimova, F. Hoffmann, G. Bekçioğlu-Neff, A. Rafferty, O. Kornilov, E. T. J. Nibbering and D. Sebastiani, *J. Am. Chem. Soc.*, 2019, **141**, 14581–14592.

7 J. R. Hunt and J. M. Dawlaty, *J. Phys. Chem. A*, 2019, **123**, 10372–10380.

8 J. R. Hunt, C. Tseng and J. M. Dawlaty, *Faraday Discuss.*, 2019, **216**, 252–268.

9 J. Lahiri, M. Moemeni, J. Kline, B. Borhan, I. Magoulas, S. H. Yuwono, P. Piecuch, J. E. Jackson, M. Dantus and G. J. Blanchard, *J. Phys. Chem. B*, 2019, **123**, 8448–8456.

10 J. Čížek, *J. Chem. Phys.*, 1966, **45**, 4256–4266.

11 J. F. Stanton and R. J. Bartlett, *J. Chem. Phys.*, 1993, **98**, 7029–7039.

12 R. S. Moog and M. Maroncelli, *J. Phys. Chem.*, 1991, **95**, 10359–10369.

13 T. Nakagawa, S. Kohtani and M. Itoh, *J. Am. Chem. Soc.*, 1995, **117**, 7952–7957.

14 W.-H. Fang, *J. Am. Chem. Soc.*, 1998, **120**, 7568–7576.

15 P.-T. Chou, C.-Y. Wei, C.-R. C. Wang, F.-T. Hung and C.-P. Chang, *J. Phys. Chem. A*, 1999, **103**, 1939–1949.

16 T. G. Kim and M. R. Topp, *J. Phys. Chem. A*, 2004, **108**, 10060–10065.

17 O.-H. Kwon, Y.-S. Lee, B. K. Yoo and D.-J. Jang, *Angew. Chem., Int. Ed.*, 2006, **45**, 415–419.

18 S.-Y. Park and D.-J. Jang, *J. Am. Chem. Soc.*, 2010, **132**, 297–302.

19 B. Kang, K. C. Ko, S.-Y. Park, D.-J. Jang and J. Y. Lee, *Phys. Chem. Chem. Phys.*, 2011, **13**, 6332–6339.

20 S.-Y. Park and D.-J. Jang, *Phys. Chem. Chem. Phys.*, 2012, **14**, 8885–8891.

21 S.-Y. Park, H.-B. Kim, B. K. Yoo and D.-J. Jang, *J. Phys. Chem. B*, 2012, **116**, 14153–14158.

22 Y. Cui, H. Zhao, J. Zhao, P. Li, P. Song and L. Xia, *New J. Chem.*, 2015, **39**, 9910–9917.

23 F. Hoffmann, M. Ekimova, G. Bekçioğlu-Neff, E. T. J. Nibbering and D. Sebastiani, *J. Phys. Chem. A*, 2016, **120**, 9378–9389.

24 G. Angulo, G. Grampp and A. Rosspeintner, *Spectrochim. Acta, Part A*, 2006, **65**, 727–731.

25 E. P. Serjeant and B. Dempsey, *Ionisation constants of organic acids in aqueous solution*, Pergammon Press, New York, 1979.

26 W. Reeve, C. M. Erikson and P. F. Aluotto, *Can. J. Chem.*, 1979, **57**, 2747–2754.

27 A. V. Marenich, C. J. Cramer and D. G. Truhlar, *J. Phys. Chem. B*, 2009, **113**, 6378–6396.

This journal is © the Owner Societies 2020

Phys. Chem. Chem. Phys., 2020, **22**, 19613–19622 | **19621**

28 P.-G. Jönsson, *Acta Crystallogr., Sect. B: Struct. Crystallogr. Cryst. Chem.*, 1976, **32**, 232–235.

29 P. Derollez, A. Hédoux, Y. Guinet, F. Danède and L. Paccou, *Acta Crystallogr., Sect. B: Struct. Sci., Cryst. Eng. Mater.*, 2013, **69**, 195–202.

30 J. Janeček and P. Paricaud, *J. Chem. Phys.*, 2013, **139**, 174502.

31 P. Sillrén, J. Swenson, J. Mattsson, D. Bowron and A. Matic, *J. Chem. Phys.*, 2013, **138**, 214501.

32 R. Böhmer, C. Gainaru and R. Richert, *Phys. Rep.*, 2014, **545**, 125–195.

33 S. A. Cirkel and R. Boese, *Acta Crystallogr., Sect. A: Found. Crystallogr.*, 2004, **60**, s205.